ADVANCES IN ATMOSPHERIC SCIENCES, VOL. 37, AUGUST 2020, 832–846

• **Original Paper** •

Diurnal Variation in the Vertical Profile of the Raindrop Size Distribution for Stratiform Rain as Inferred from Micro Rain Radar Observations in Sumatra

Ravidho RAMADHAN[1], MARZUKI*[1], Mutya VONNISA[1], HARMADI[1], Hiroyuki HASHIGUCHI[2], and Toyoshi SHIMOMAI[3]

[1]*Department of Physics*, *Andalas University*, *Padang* 25163, *Indonesia*

[2]*Research Institute for Sustainable Humanosphere (RISH)*, *Kyoto University*, *Uji*, *Kyoto* 611-0011, *Japan*

[3]*Remote Sensing Laboratory*, *Interdisciplinary Faculty of Science and Engineering*
Shimane University, *Matsue* 690-0823, *Japan*

(Received 28 August 2019; revised 12 April 2020; accepted 29 April 2020)

ABSTRACT

The diurnal variation in the vertical structure of the raindrop size distribution (RSD) associated with stratiform rain at Kototabang, West Sumatra (0.20°S, 100.32°E), was investigated using micro rain radar (MRR) observations from January 2012 to August 2016. Along with the MRR data, the RSD from an optical disdrometer and vertical profile of precipitation from the Tropical Rainfall Measuring Mission were used to establish the microphysical characteristics of diurnal rainfall. Rainfall during 0000–0600 LST and 1800–2400 LST had a lower concentration of small drops and a higher concentration of large drops when compared to rainfall during the daytime (0600–1800 LST). The RSD stratified on the basis of rain rate (R) showed a lower total concentration of drops and higher mass-weighted mean diameter in 0000–0600 LST and 1800–2400 LST than in the daytime. During the daytime, the RSD is likely governed by a riming process that can be seen from a weak bright band (BB). On the other hand, during 0000–0600 LST and 1800–2400 LST, the BB was stronger and the rainfall was associated with a higher concentration of midsize and large drops, which could be attributed to more active aggregation right above the melting layer with minimal breakup. Diurnal variation in the vertical profile of RSD led to a different radar reflectivity (Z)–R relationship in the rain column, in which Z during the periods 0000–0600 LST and 1800–2400 LST was larger than at the other times, for the same R.

Key words: diurnal variation, raindrop size distribution, micro rain radar, stratiform rain, Kototabang

Citation: Ramadhan, R., Marzuki, M. Vonnisa, Harmadi, H. Hashiguchi, and T. Shimomai, 2020: Diurnal variation in the vertical profile of the raindrop size distribution for stratiform rain as inferred from micro rain radar observations in Sumatra. *Adv. Atmos. Sci.*, **37**(8), 832−846, https://doi.org/10.1007/s00376-020-9176-9.

Article Highlights:

- Differences in the RSD of diurnal rainfall at Kototabang were found.
- The concentration of RSD was higher in the afternoon (1200–1800 LST), during which a relatively high concentration of small raindrops was found.
- A vertically downward decrease in coefficient A of the Z–R relationship was obvious; the smallest value near the surface was observed during 1200–1800 LST.
- Riming is the likely dominant process in the afternoon, whereas aggregation is dominant in the morning.
- Estimation of the R using a fixed Z–R relation can result in large errors, even for stratiform rain.

1. Introduction

The diurnal cycle is one of the main components of atmospheric variation in the tropics, as a result of atmosphere–ocean–land interactions in response to solar radiation. In general, the amplitude of diurnal cycles on land is much larger than in ocean areas. On land, rainfall peaks tend to occur in the afternoon, while over oceans they tend to occur in the morning (Albright et al., 1981; Hamilton, 1981; Yang and Slingo, 2001; Tian et al., 2004). However, owing to the interaction of many factors, diurnal cycles can vary from one

* Corresponding author: MARZUKI
Email: marzuki@sci.unand.ac.id

region to another. The rainfall peak in the afternoon is not only observed on land but also seen over oceans, such as in the eastern tropical Atlantic (Albright et al., 1985), the South Pacific convergence zone (Sui et al., 1997), and the middle and eastern tropical Pacific (Augustine, 1984). High rainfall peaks have also been observed in coastal areas—for example, in Sumatra—owing to the propagation of the rainfall peak from land, due to the movement of land–sea winds (Mori et al., 2004).

In addition to rainfall patterns, diurnal variation also affects the microstructure of precipitation, such as the raindrop size distribution (RSD), which can influence the accuracy of rainfall estimated using weather radar (Kozu et al., 2006). Different microphysical processes experienced by raindrops during the day and night in response to the difference in the intensity of solar radiation may generate different RSD characteristics on the ground (Radhakrishna et al., 2009). Kozu et al. (2006) observed strong diurnal variations in the RSD at Kototabang (Sumatra) and Gadangki (India) that were generated by land–ocean interaction. Marzuki et al. (2009, 2013a, 2016a) also observed diurnal variation in the RSD at Kototabang. Recently, Nauval et al. (2017) observed diurnal variation in the RSD at several locations in Indonesia. A typical picture of the diurnal cycle of a tropical RSD derived from previous observational studies is as follows: the RSDs in the morning hours of 0000–1200 LST are narrower than those in the evening (1200–2400 LST). The diurnal variations in the RSD lead to significant variation in radar reflectivity (Z)–rainfall rate (R) relations. Local convection in the afternoon plays an important role in generating a broader RSD (Kozu et al., 2006). Diurnal variations in the RSD are less observed in areas where the RSD is strongly influenced by the oceanic nature of rainfall, such as in Singapore (Kozu et al., 2006). Ushiyama et al. (2009) and Marzuki et al. (2018a) also observed weak diurnal variation in the RSD in Palau and over the Indian Ocean, respectively.

While there have been several studies on the diurnal variation in the RSD, such studies have mostly dealt with the diurnal variation in the RSD at the ground surface. To understand the microphysical process experienced by the RSD during a rain event, it is necessary to observe the vertical structure of the RSD on a diurnal basis. Furthermore, the vertical structure of the RSD is also important for latent heat studies and rainfall estimates that are obtained using weather radar (Li and Srivastava, 2001; Kumjian and Ryzhkov, 2010).

This work investigated the vertical structure of the RSD at Kototabang, West Sumatra (0.20°S, 100.32°E), using a micro rain radar (MRR). Studies have been conducted on the vertical structure of the RSD at Kototabang (Kozu et al., 2005; Renggono et al., 2006; Marzuki, 2010). However, such studies only investigated the intraseasonal variation in the vertical profile of the RSD. Furthermore, the RSD was retrieved from a 47-MHz equatorial atmospheric radar (EAR), which is less sensitive to precipitation particles (Fukao et al., 2003). To overcome the limitations of previous studies, we analyzed data collected by an MRR—an instrument that operates at a frequency of 24 GHz, meaning it is strongly attenuated by raindrops during heavy rain. The measured spectra of an MRR can also suffer from aliasing errors, due to strong vertical winds. However, as long as the vertical wind is lower than 2 m s^{-1}, the instrument can provide good estimates of the actual RSD, and hence the retrieved rain parameters (Peters et al., 2005). The vertical wind during stratiform rain at Kototabang is generally smaller than 1 m s^{-1} (Marzuki et al., 2016a). Therefore, this work was limited to stratiform rain, which generally has an intensity of less than 10 mm h^{-1}. Although not all types of rain are discussed in this paper, in the tropics, stratiform rain contributes to 73% of the area covered by rain and around 40% of the total rain amount (Schumacher and Houze, 2003). Thus, this research can serve as an important additional reference on the vertical structure of raindrops in the tropics, especially at Kototabang.

2. Data and methods

2.1. *Site and instruments*

The experiment was conducted at the Equatorial Atmosphere Observatory (EAO), which is located in Kototabang, West Sumatra, Indonesia (0, 20°S, 100, 32°E; 865 m above sea level). The experimental site lies in an equatorial zone that has two rainy seasons, in March–May and September–December (Aldrian and Dwi Susanto, 2003; Marzuki et al., 2016b). The average annual rainfall from an 11-year rain gauge observation at Kototabang was 2532 ± 355 mm yr^{-1} (Marzuki et al., 2016b).

The RSD profile data were recorded by a vertically pointing MRR. The MRR is a frequency modulated continuous wave (FMCW) Doppler radar that is competitive with pulse radars with regard to range resolution when the same signal bandwidth is used. Unlike radars that detect the time delay of the returned pulse, most FMCW radars base their measurements on differences in instantaneous frequency between the received and transmitted signals. A detailed description of the MRR can be found in Peters et al. (2005).

Briefly, the RSD of the MRR is estimated using the spectral reflectivity density $\eta(D)$, which is divided by the single particle backscattering cross section $\sigma(D)$ of a rain drop of diameter D:

$$N(D) = \frac{\eta(D)}{\sigma(D)}, \tag{1}$$

where $\eta(D)$ is given by

$$\eta(D) = 6.18\eta(v)e^{-0.6D}\delta v(h). \tag{2}$$

The value of $\eta(v)$ in Eq. (2) is the $\eta(D)$ with respect to velocity, and $\delta v(h)$ is a height-dependent density correction for the fall velocity given by Peters et al. (2005):

$$\delta v(h) = 1 + 3.68 \times 10^{-5} h + 1.71 \times 10^{-9} h^2 . \quad (3)$$

Equation (2) is applied only in the raindrop size range 0.246 mm $\leqslant D \leqslant$ 5.03 mm. From the RSD, Z, R and the liquid water content (LWC) are computed as follows:

$$Z = \int_{D_{\min}}^{D_{\max}} N(D) D^6 \mathrm{d}D ; \quad (4)$$

$$R = \frac{\pi}{6} \int_{D_{\min}}^{D_{\max}} N(D) v(D) D^3 \mathrm{d}D ; \quad (5)$$

$$\mathrm{LWC} = \rho_w \frac{\pi}{6} \int_{D_{\min}}^{D_{\max}} N(D) D^3 \mathrm{d}D , \quad (6)$$

where ρ_w is the density of water, and $v(D)$ is the terminal falling velocity given by Atlas et al. (1973):

$$v(D) = 9.65 - 10.3 e^{-0.6D} \delta v(h) . \quad (7)$$

The MRR at Kototabang has 31 range gates with a resolution of 150 m (Table 1). Thus, the altitudinal coverage of this instrument is 0.15–4.65 km above ground level (AGL). Owing to the noise and ground clutter (Peters et al., 2005), we excluded the data for altitudes lower than 300 m. The MRR installed at Kototabang shows good performance, particularly for $R < 10$ mm h^{-1} (Marzuki et al., 2016c). We analyzed the data from January 2012 to August 2016 (1549 days), with a temporal resolution of one minute. There is an optical rain gauge (ORG) at the EAO. We only analyzed the MRR data if the R at the ground surface recorded by the ORG was more than 0.1 mm h^{-1}. Simultaneous observations of the MRR and the ORG provided 8528 min of data.

This study also used RSD data from PARSIVEL (particle size velocity) optical disdrometer observations during 2012–16. The Z–R relation derived from the MRR was compared with that governed by using the RSD from PARSIVEL observations. There are some limitations of PARSIVEL, such as the limited sampling area, spherical raindrop assumption, and the possibility to have multiple drops passing through the sampling area at the same time (e.g., Tokay et al., 2013). Nevertheless, PARSIVEL is a low cost, durable, and reliable instrument, so it is widely used. We applied several quality control procedures to minimize the measurement error of PARSIVEL. The data from the first two size bins were discarded, and thus we constructed the RSD at 1-min intervals from 0.3 to 10 mm. We also disregarded very light rain ($R < 0.1$ mm h^{-1}) and minutes with fewer than 10 drops. Additionally, we adopted a threshold of fall speed using Atlas' empirical velocity [Eq. (7)] and retained the drops within ± 60% of the empirical velocity. All quality control procedures have been used in some previous works based on Kototabang data, such as in Marzuki et al. (2013b). Recently, Marzuki et al. (2018c) showed the accuracy of PARSIVEL at Kototabang to measure rainfall, by comparing the daily rainfall with that obtained by ORG. In this study, we also used ORG to evaluate the performance of PARSIVEL. We only analyzed PARSIVEL data if daily rainfall from PARSIVEL was in good agreement with the rainfall from ORG. Simultaneous observations of the MRR, ORG, and PARSIVEL provided 7020 min of data.

In addition to vertical profile of Z from the MRR, that from the Tropical Rainfall Measuring Mission (TRMM) 2A25-Precipitation Radar product over a four-year time span (2012–15) was also used, to discuss the possible microphysical processes affecting the RSD during the falling of raindrops to the ground. Only the TRMM 2A25 profiles with an incidence angle of less than 7° on either side of nadir were used (Geerts and Dejene, 2015; Marzuki et al., 2018d).

Table 1. Specification of the MRR at Kototabang.

Radar parameters	Specification
Radar system	FMCW
Operating frequency	24.1 GHz
Transmit power	50 mW
Antenna	60 cm in diameter
Beam width	2°
Range resolution	150 m
Time resolution	60 s
Range gates	31
Observation period	January 2012–August 2016

2.2. *Methods*

Stratiform rain was extracted from the MRR data based on the existence of a melting layer or bright band (BB). Several methods can be used to detect the BB from the MRR data, but we used the gradient of falling velocity (GVF) as the BB indicator, following the method proposed by Wang et al. (2017). The accuracy of this method was determined visually for each profile in such a way that the stratiform rain was marked by the appearance of the BB. Figure 1 shows the height distribution of the 8528-min data that were classified as stratiform. The existence of a BB can be observed clearly from the Z, falling velocity and LWC. The BB top varied, but generally it lay at 4.05 km, which is consistent with previous research on the melting layer height at Kototbang. Marzuki et al. (2013a) classified precipitation at Kototabang using wind profilers and found the melting layer height to be around 4 km AGL. Recently, Marzuki et al. (2018b) analyzed the climatology of the melting layer at Kototabang using 17 years of TRMM 2A25 data and found the average annual melting layer height to vary from 3.92 to 4.11 km AGL. The melting layer heights from radars were also consistent with the 0°C isotherm level derived from the average temperature profile from radiosonde observations (figure not shown).

The data were classified into several R categories—

namely, very light ($0.1 \leqslant R < 1$ mm h^{-1}), light ($1 \leqslant R < 2$ mm h^{-1}), moderate ($2 \leqslant R < 5$ mm h^{-1}), and heavy ($5 \leqslant R < 10$ mm h^{-1}) stratiform rain; plus, four non-overlapping LST time spans—namely, 0000–0600, 0600–1200, 1200–1800, and 1800–2400 LST, following Kozu et al. (2006). Table 2 summaries the distribution of the data for each category.

The RSD was parameterized by the modified gamma distribution (Kozu and Nakamura, 1991; Tokay and Short,

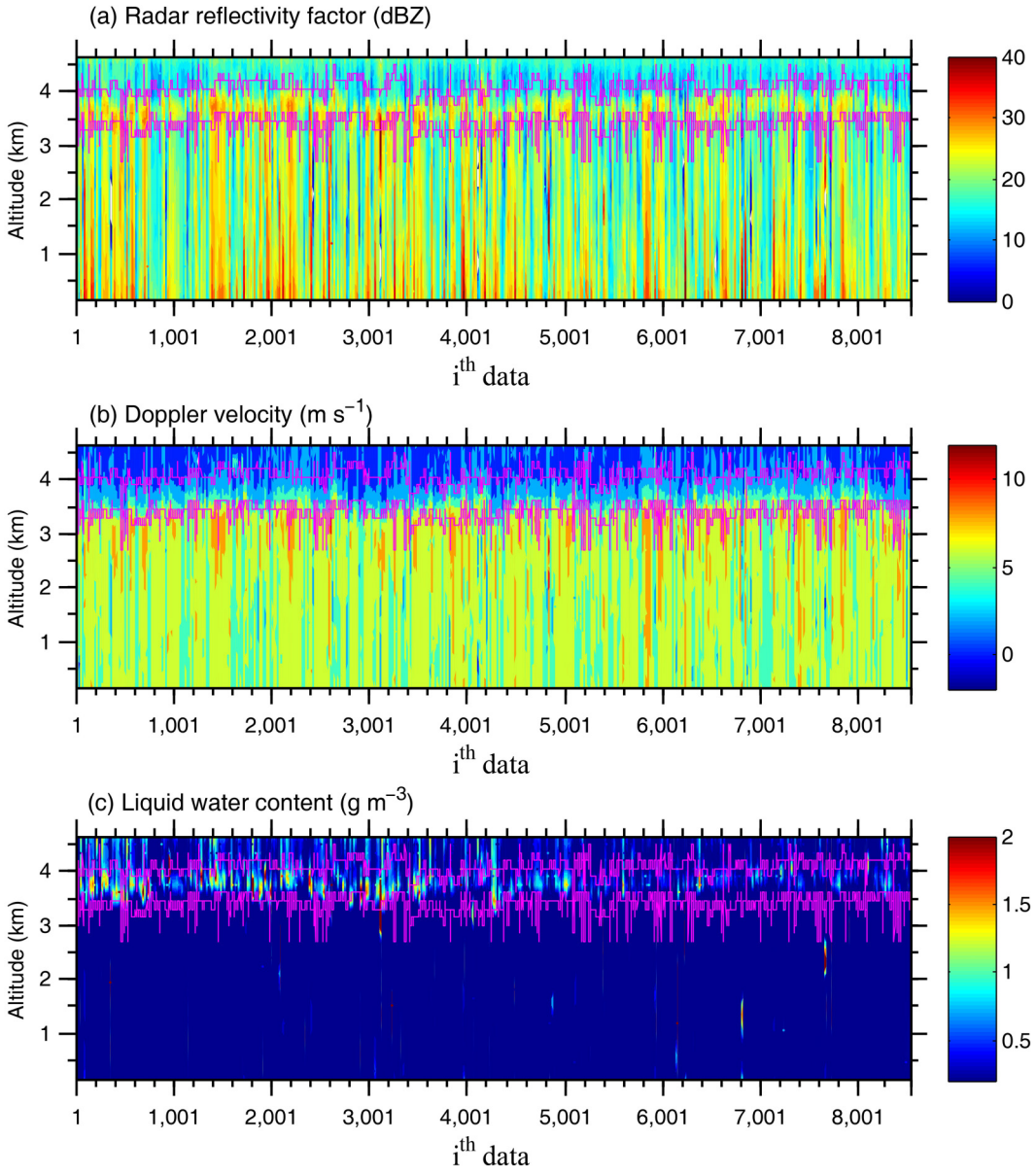

Fig. 1. Height distribution of 8528 min of data classified as stratiform rain from simultaneous observations of the MRR and ORG, for (a) Z, (b) falling velocity, and (c) LWC. The purple lines indicate the BB bottom and top heights.

Table 2. Distribution of data for several R categories on a diurnal basis.

Time	Number of data for several rainfall categories			
	Very light rain ($0.1 \leqslant R < 1$ mm h^{-1})	Light rain ($1 \leqslant R < 2$ mm h^{-1})	Moderate rain ($2 \leqslant R < 5$ mm h^{-1})	Heavy rain ($5 \leqslant R < 10$ mm h^{-1})
0000–0600 LST	2255	464	208	31
0600–1200 LST	331	108	40	-
1200–1800 LST	1065	266	105	37
1800–2400 LST	2433	721	269	13

1996), which is given by

$$N(D) = N_T \frac{\Lambda^{\mu+1} D^{\mu}}{\Gamma(\mu+1)} e^{-\Lambda D}, \quad (8)$$

where $N(D)$ is the RSD (units: m^{-3} mm^{-1}), N_T is the total raindrop concentration (units: m^{-3}), μ is the shape parameter, Λ is the slope (units: mm^{-1}), $\Gamma(x)$ is the complete gamma function, and D is the raindrop diameter (units: mm). The parameters of the gamma RSD were calculated by the moment method. In this work, we used the moments of M_3, M_4 and M_6, as integral rainfall parameters for remote sensing applications are mainly proportional to these moments (Kozu and Nakamura, 1991). Each gamma RSD parameter was obtained as follows (Tokay and Short, 1996):

$$N_T = \frac{\Lambda^3 M_3 \Gamma(\mu+1)}{\Gamma(\mu+4)}; \quad (9)$$

$$\Lambda = \frac{\mu+4}{D_m}; \quad (10)$$

$$\mu = \frac{11G - 8[G(G+8)]^{1/2}}{2(1-G)}; \quad (11)$$

$$G = \frac{M_4^3}{M_3^2 M_6}, \quad (12)$$

where D_m is the mass-weighted mean diameter, which is expressed by

$$D_m = \frac{M_4}{M_3}. \quad (13)$$

Weather radars usually estimate the R from the Z data using a Z–R relation. The empirical Z–R relation is a power law form given by

$$Z = AR^b, \quad (14)$$

where A and b are unknown constants. These constants are dependent on the shape of the RSD. In this study, the linear regression between Z and R on a logarithmic scale governs the Z–R relation. The sequential intensity filtering technique (Lee and Zawadzki, 2005) was used to reduce the spurious variability of the MRR and PARSIVEL data.

3. Results

3.1. *Vertical profile of average RSD*

Figure 2 shows the vertical profile of the RSD for several R categories. Above 3 km AGL, the concentration of small-sized drops ($D < 0.5$ mm) was very high [$N(D) > 10^4$ m^{-3} mm^{-1}], and this contributed to the high value of LWC (Fig. 1c). In general, the growth of raindrops was observed throughout the day, but the growth during 0000–0600 LST was stronger than that during other times. For very light rain (0.1–1 mm h^{-1}), and at altitudes of 0.45–3 km AGL (Figs. 2a–d), during the periods 0000–1200 LST and 1800–2400 LST, raindrops with sizes larger than 1 mm tended to be constant or grow slightly with height. For D = 2 mm, the RSD on a logarithmic scale at 3 (0.6 km) for the periods 0000–0600, 0600–1200, 1200–1800 and 1800–2400 LST was 0.005 (0.29), −0.2013 (0.17), 0.097 (0.50) and 0.12 (0.39) m^{-3} mm^{-1}, respectively. For D = 0.5 mm, the RSD on a logarithmic scale at 3 (0.6 km) for 0000–0600, 0600–1200, 1200–1800 and 1800–2400 LST was 2.45 (2.58), 2.54 (2.53), 2.82 (2.89) and 2.62 (2.36) m^{-3} mm^{-1}, respectively. Thus, a slight increase in the concentration of small sized-drops ($D < 0.5$ mm) with height was also observed, except during the period 1800–2400 LST. This condition was also clearly illustrated by the average RSD value for several heights (Fig. 3).

For higher R, the diurnal variation in raindrop growth was more significant (Figs. 2e–p). There were no data for the heavy rain category during 0600–1200 LST. During this period, precipitation was seldom observed at Kototabang (Marzuki et al., 2016b). For heavy rain (5–10 mm h^{-1}), as for very light rain, the concentration of small-sized drops ($D < 0.5$ mm) above 3 km AGL was very high [$N(D) > 10^4$ m^{-3} mm^{-1}]. For an altitude of 0.45–3 km AGL, during 0000–0600 LST, raindrops underwent significant growth (Fig. 2m). For example, for D = 2 mm, the RSD on a logarithmic scale at 3 (0.6 km) for the periods 0000–0600, 1200–1800 and 1800–2400 LST was −0.087 (0.28), 0.31 (0.35) and 0.12 (0.29) m^{-3} mm^{-1}, respectively. Furthermore, a decrease in the concentration of small sized-drops ($D <$ 0.5 mm) with height was also observed for all time periods except during 1800–2400 LST. At 3 km, the RSD of 0.5-mm raindrops on a logarithmic scale for the periods 0000–0600, 1200–1800 and 1800–2400 LST was 2.51, 2.74 and 2.28 m^{-3} mm^{-1}, respectively, and the values decreased or increased to 2.11, 2.62 and 2.63 m^{-3} mm^{-1} at 0.6 km. This feature was more clearly illustrated by the average RSD value for several heights (Fig. 4). The downward increase in the concentration of large-sized raindrops ($D > 2$ mm) coincided with the downward decrease in the concentration of small-sized raindrops ($D < 0.5$ mm). Thus, coalescence may be the dominant microphysical process for this R category (Rosenfeld and Ulbrich, 2003). This is quite surprising because collision–coalescence is generally unimportant at R values lower than about 25 mm h^{-1} (Hu and Srivastava, 1995).

3.2. *Vertical profile of RSD parameters*

Figure 5 shows the vertical structure of the gamma RSD. In general, a downward increase in μ and D_m and a downward decrease in N_T were clearly observed. For very light rain (Figs. 5a–c), the μ at 3 (0.45 km) for the periods 0000–0600, 0600–1200, 1200–1800 and 1800–2400 LST was −2.70 (−1.54), −2.49 (−1.61), −2.79 (−1.62) and −2.73 (−1.15), respectively. Furthermore, the D_m at 3 (0.45 km) was 0.69 (1.21), 0.63 (0.99), 0.63 (1.13) and 0.69 (1.34)

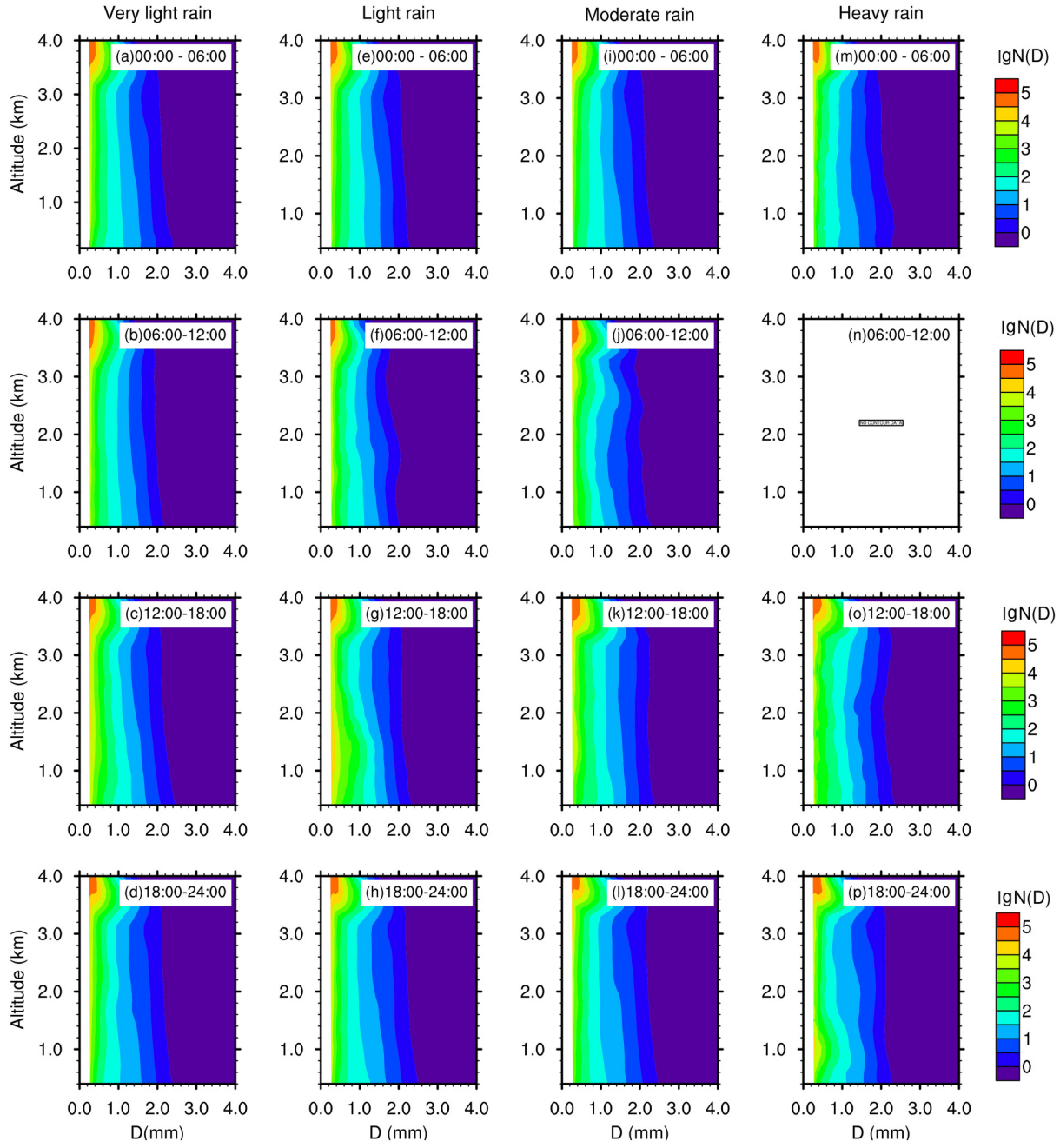

Fig. 2. . Diurnal variation in the average vertical profile of the RSD for very light ($0.1 \leqslant R < 1$ mm h^{-1}), light ($1 \leqslant R < 2$ mm h^{-1}), moderate ($2 \leqslant R < 5$ mm h^{-1}), and heavy ($5 \leqslant R < 10$ mm h^{-1}) stratiform rain. There were no data during 0600–1200 LST for the heavy rain category.

mm. Thus, the D_m for 0600–1200 LST at the ground was smaller than that at the other times, indicating a smaller number of large drops, which is consistent with Fig. 2. The largest N_T was observed during the period 1200–1800 LST. The N_T at 3 (0.45 km) for the periods 0000–0600, 0600–1200, 1200–1800 and 1800–2400 LST was 2384 (797), 2488 (1089), 3843 (1516) and 2711 (638) m^{-3}, respectively.

All the RSD gamma parameters near the ground surface from stratiform rain varied with R. The value of the RSD gamma parameter associated with heavy rain (Figs. 5j–l) was slightly larger than that of very light rain (Figs. 5a and b). This is typical of RSD characteristics in the tropics (Tokay and Short, 1996; Marzuki et al., 2010, 2013a). For heavy rain, parameter μ at 3 (0.45 km) for the periods 0000–0600, 1200–1800 and 1800–2400 LST was −2.68 (−1.09), −2.45 (−1.16) and −2.71 (−1.30), respectively. The smallest μ at the ground surface was observed during the period 1200–1800 LST, indicating a high concentration of small drops. The D_m at 3 (0.45 km) was 0.64 (1.47), 0.75 (1.10) and 0.71 (1.13) mm. Thus, the D_m at the ground for the period 1200–1800 LST was smaller than that at the

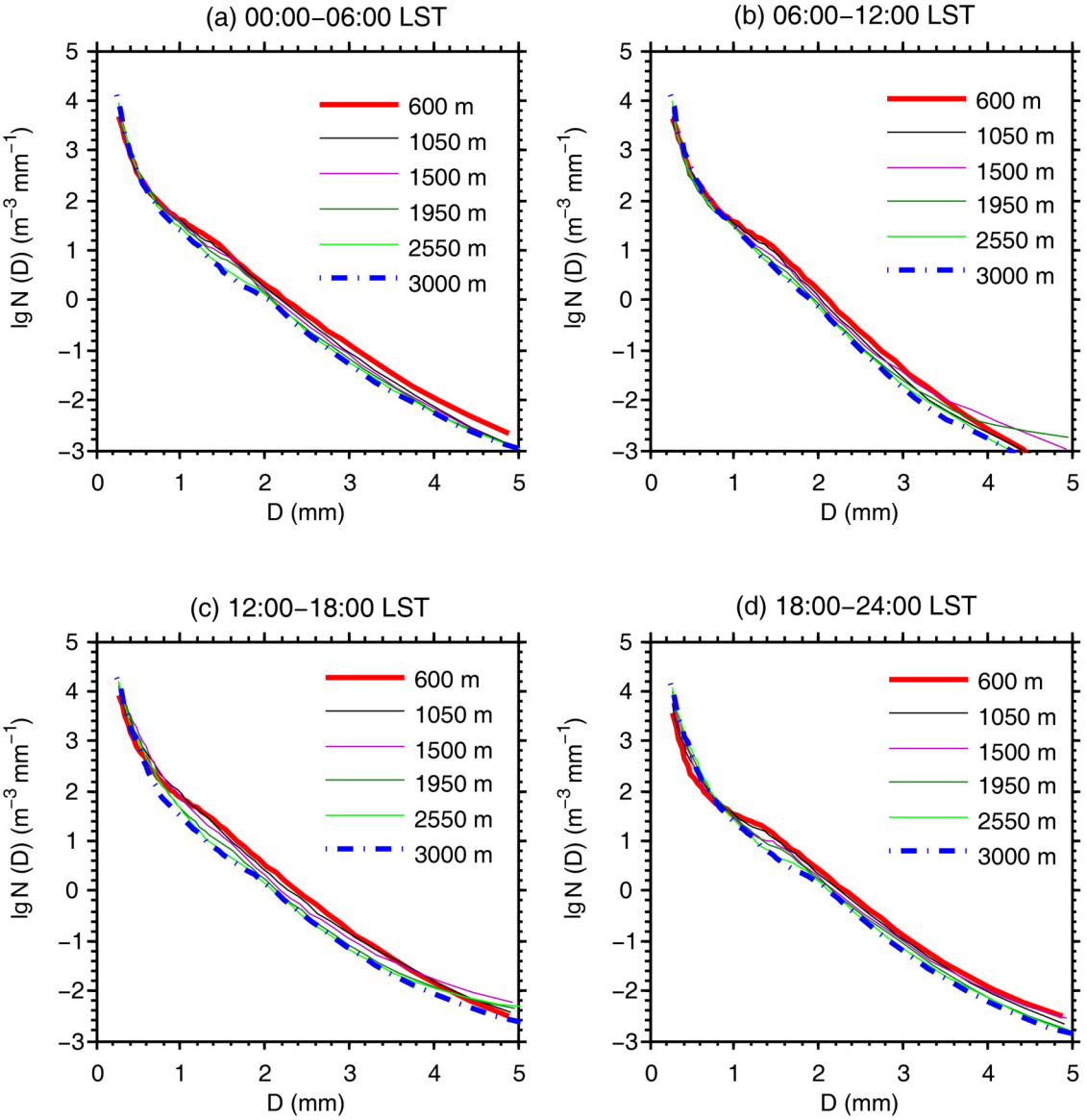

Fig. 3. Diurnal variation in the average RSD for several heights for very light rain (0.1–1 mm h^{-1}).

other times, indicating a smaller number of large drops, which is consistent with Fig. 2. The N_T at 3 (0.45 km) for the periods 0000–0600, 1200–1800 and 1800–2400 LST was 2596 (336), 4159 (1121) and 2261 (854) m^{-3}, respectively. Thus, the largest N_T throughout the rain column (0.45–3 km) was observed during the period 1200–1800 LST.

The aforementioned results show that the diurnal variation in the RSD of stratiform rain is obvious. The highest drop concentration (N_T) was observed during the period 1200–1800 LST, and the RSD in this period contained a large number of small drops and a small number of large drops, such that the μ and D_m were smaller at the surface. The smaller number of large drops of stratiform rain during the period 1200–1800 LST, as indicated by the small D_m (Figs. 5c, f, i and l), resulted in a smaller Z at the surface during this period (Fig. 6), except for heavy rain (Fig. 6d). This is different to convective rain, for which large Z values are frequently observed during the period 1200–1800 LST, indicating intense convection (Marzuki et al., 2016a). Note that the GVF was used as the BB indicator in this work. Although the BB is not very clear in Fig. 6d, the vertical profile of the falling velocity shows the occurrence of a BB for all rainfall intensities (Fig. 7).

The BB strength plays an important role in determining the number and size of raindrops (Wang et al., 2017). To see the strength of BB (ΔZ), we calculated ΔZ by averaging the reflectivity gradient within the BB (Huggel et al., 1996). Figure 8 is a 2D scatterplot between the D_m and ΔZ. The linear regression equation between the two parameters for the periods 0000–0600, 0600–1200, 1200–1800 and 1800–2400 LST was $D_m = 0.101\Delta Z + 0.653$ ($r = 0.37$), $D_m = 0.040\Delta Z + 0.879$ ($r = 0.21$), $D_m = 0.054\Delta Z + 0.923$ ($r = 0.20$) and $D_m = 0.108\Delta Z + 0.744$ ($r = 0.36$), respectively. Thus, the relationship between D_m and ΔZ during 0000–0600 and 1800–2400 LST was stronger than that dur-

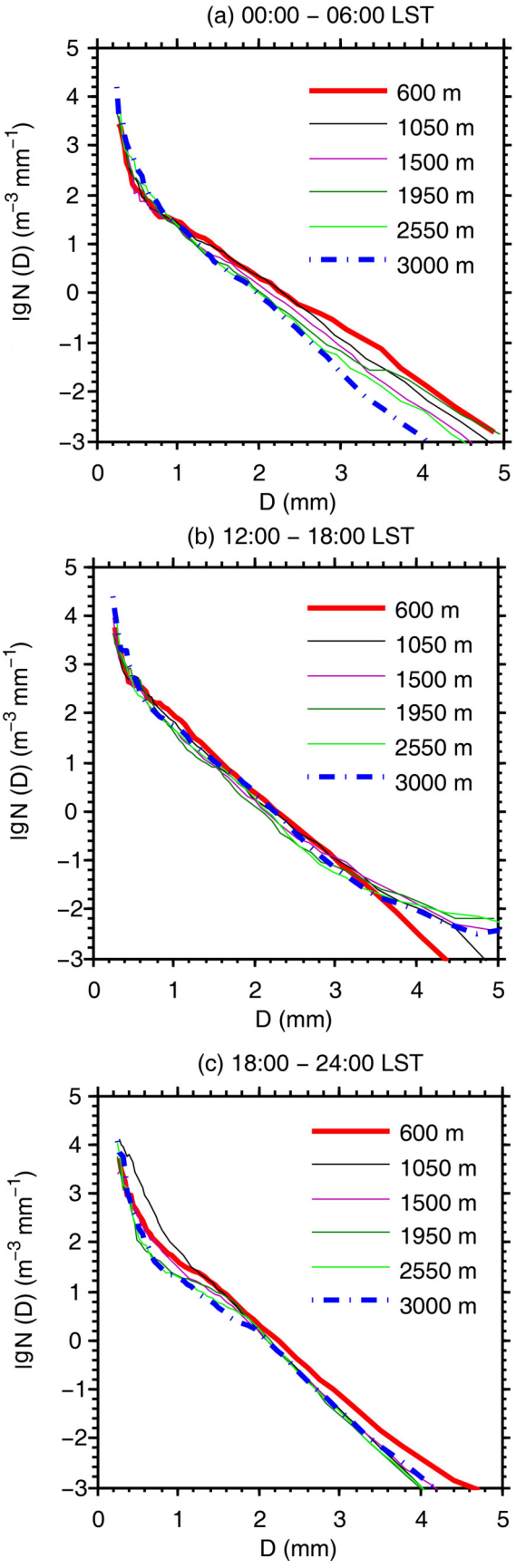

Fig. 4. Diurnal variation in the average RSD for several heights for heavy rain (5–10 mm h^{-1}). There were no data during 0600–1200 LST for this rain category.

ing other periods. If the four equations are plotted together, we can see clearly that, for the same ΔZ, the value of D_m during 0000–0600 and 1800–2400 LST was larger than that during 0600–1800 LST.

The characteristics of the diurnal variation in the BB from the MRR were consistent with those obtained from the TRMM 2A25 data. We calculated the strength of the BB at Kototabang using the TRMM data during 2012–15. For very light rain (R < 1 mm h^{-1}), the ΔZ for the periods 0000–0600, 0600–1200, 1200–1800 and 1800–2400 LST was 3.86, 2.85, 2.85 and 4.05 dBZ, respectively. Furthermore, the ΔZ for heavy rain (5–10 mm h^{-1}) was 4.09, 2.46, 2.48 and 3.53, respectively. Thus, during the daytime (1200–1800 LST), the BB was weaker than at other times, and the RSD was number controlled, which is governed predominantly by a riming process (Sarma et al., 2016). A weak BB during 1200–1800 LST is associated with many small drops (Huggel et al., 1996), which can be also seen from the large N_T and small D_m. On the other hand, during the periods 1800–2400 LST and 0000–0600 LST, the BB was stronger, and a strong BB is associated with larger drops (large D_m), which are attributable to more active aggregation right above the melting layer (Fabry and Zawadzki, 1995; Huggel et al., 1996; Zawadzki et al., 2005).

3.3. *Vertical profile of the Z–R relation*

Figure 9 shows the vertical profiles of coefficients A and b of the Z–R relation on a diurnal basis for stratiform rain at Kototabang. In general, coefficient A increased with decreasing height, while b decreased. This feature is similar to typical values of A and b for stratiform rain (Cifelli et al., 2000). The Z–R at the altitude of 3.0 km was $Z = 424R^{1.83}$, which changed to $Z = 433R^{1.25}$ near the surface (0.45 km). The Z–R relation of the near surface was close to that obtained from the PARSIVEL data ($Z = 413R^{1.29}$) at the ground level. Thus, coefficients A and b were not constant for each altitude, so the use of the Marshall–Palmer relation—namely, $Z = 200R^{1.6}$—for each height, can affect the accuracy of the rain estimate using weather radar observations.

Coefficient A and exponent b showed a significant diurnal variation as a result of the variation in the RSD. At the near surface (0. 45 km), coefficient A (b) for the time periods 0000–0600, 0600–1200, 1200–1800 and 1800–2400 LST was 456 (1.35), 352 (1.25), 346 (1.18) and 482 (1.26), respectively. A similar pattern was also observed from the PARSIVEL data, in which coefficient A (b) for the aforementioned periods, respectively, was 379 (1.34), 322 (1.23), 379 (1.31) and 465 (1.29). For the same R, the Z–R relationships derived from both the MRR and PARSIVEL data resulted in a slightly larger Z during 0000–0600 and 1800–2400 LST than the other time periods, which is consistent with Fig. 6. Coefficient A is the intercept of the Z–R relation line and it is determined by the shape of the RSD and in particular from the Z. A large value for coefficient A is associated with more large-sized drops, leading to larger Z and D_m values for the same R. Thus, for the same R, the RSD of strati-

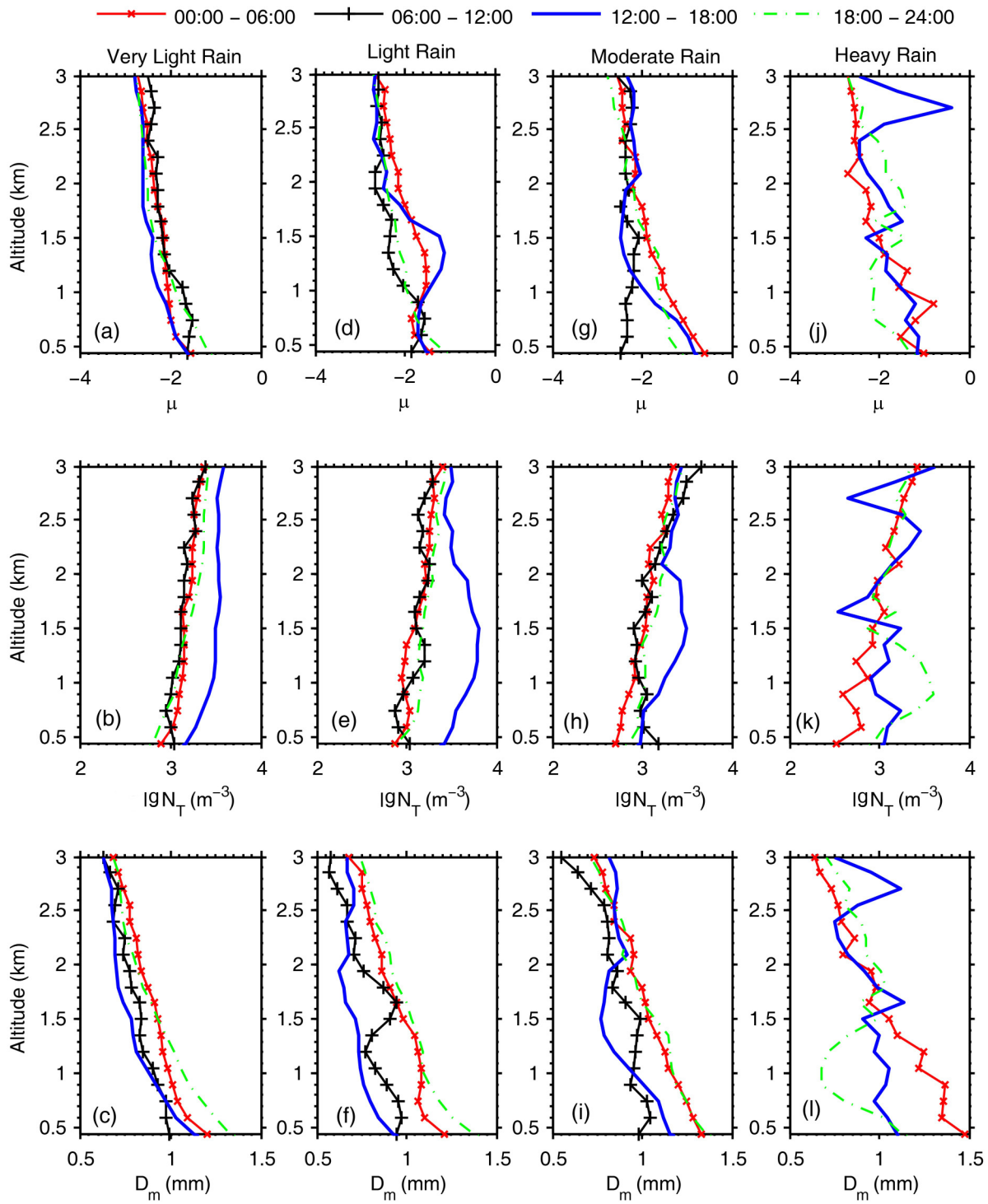

Fig. 5. Average RSD gamma parameters for (a) very light ($0.1 \leqslant R < 1$ mm h^{-1}), (b) light ($1 \leqslant R < 2$ mm h^{-1}), (c) moderate ($2 \leqslant R < 5$ mm h^{-1}), and (d) heavy ($5 \leqslant R < 10$ mm h^{-1}) stratiform rain. There were no data during 0600–1200 LST for the heavy rain category.

form rain for the time period 1200–1800 LST had a smaller number of large drops than that for the other time periods. However, the total concentration of raindrops during the period 1200–1800 LST was much higher than at the other times (Fig. 5).

Coefficient A during the day (1200–1800 LST) was smaller than during the other periods, throughout the rain column (0.45–3 km). Its value at 3 (1.5 km) for the periods 0000–0600, 0600–1200, 1200–1800 and 1800–2400 LST was 406 (351), 223 (338), 381 (243) and 505 (497), respectively. During the daytime, the BB was weaker than at other times, and a weak BB is associated with smaller drops, due to the riming process of snow that leads to smaller Z and A values. On the other hand, during 0000–0600 and

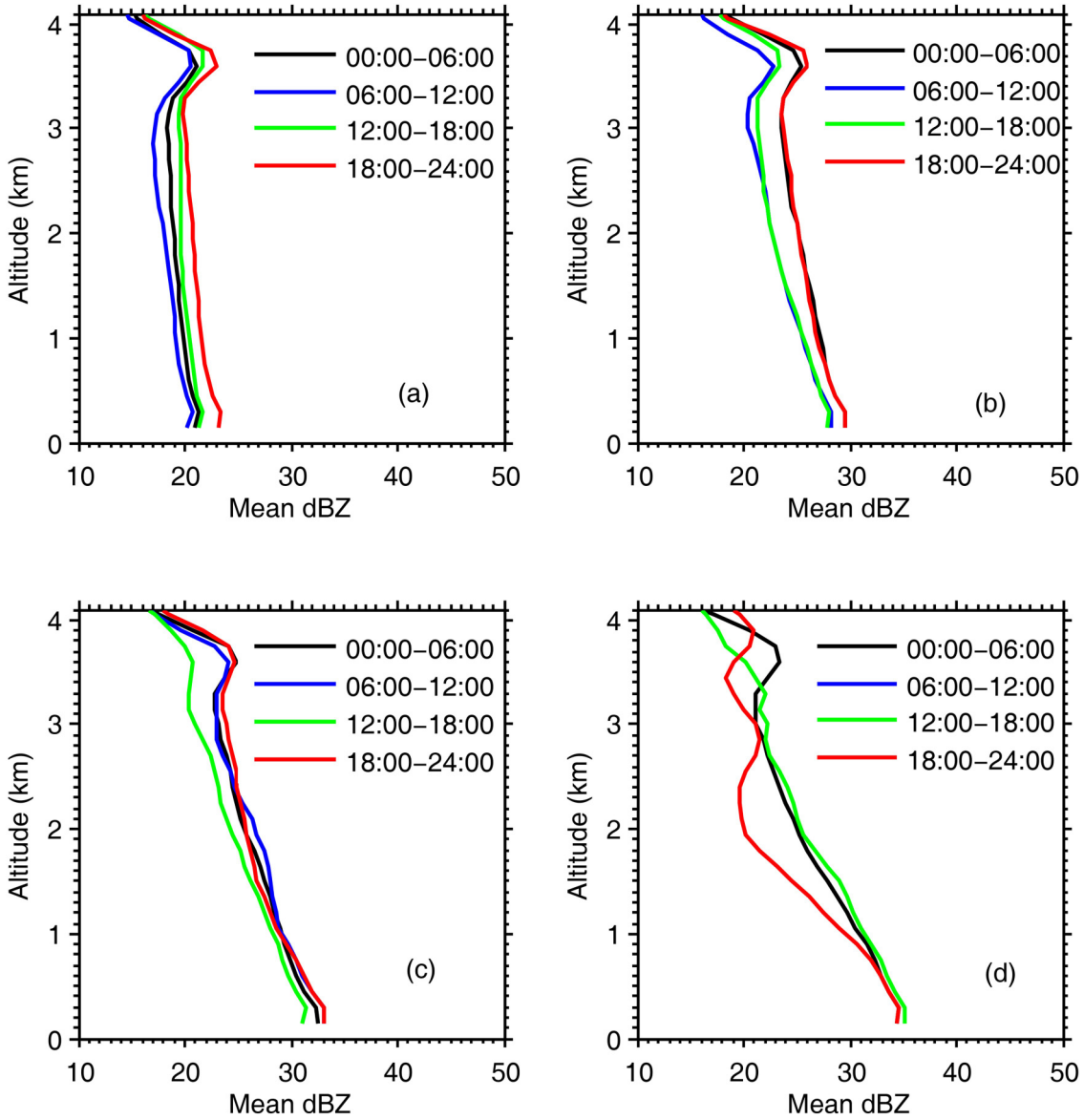

Fig. 6. Average Z from the MRR for (a) very light ($0.1 \leqslant R < 1$ mm h^{-1}), (b) light ($1 \leqslant R < 2$ mm h^{-1}), (c) moderate ($2 \leqslant R < 5$ mm h^{-1}), and (d) heavy ($5 \leqslant R < 10$ mm h^{-1}) stratiform rain. There were no data during 0600–1200 LST for the heavy rain category.

1800–2400 LST, the BB was stronger than at other times, which indicates the appearance of more active aggregation right above the melting layer (Fabry and Zawadzki, 1995; Huggel et al., 1996; Zawadzki et al., 2005). Besides the strength of the BB, variation in the melting layer height can also affect the RSD at the ground because it is closely related to aggregation and riming above the melting layer and drop sorting and collision coalescence below the melting layer (Rosenfeld and Ulbrich, 2003). However, the difference in the melting layer height for each time period at Kototabang was small (~100 m) (Fig. 10) and may not have caused any significant difference in the RSD. A small variation in the melting layer height was also observed by the MRR (Fig. 6). The mean BB top height from MRR observations for 0000–0600, 0600–1200, 1200–1800 and 1800–2400 LST was 4.06, 3.99, 4.10 and 4.11 km, respectively.

Because the values of b and A decrease and increase with decreasing height, respectively, the microphysical processes that affect the raindrop growth of stratiform rain at Kototabang are evaporation and coalescence (Wilson and Brandes, 1979). Evaporation is dominant for light rain and collision–coalescence is dominant for heavy rain. A breakup process can also cause an increase in the number of small drops and a decrease in the number of large drops. However, if breakup occurs, there must be a consequent decrease in D_{m} and an increase in N_{T}. Furthermore, there must be a small change in μ with a tendency towards a decrease. The end result of the breakup process is a decrease in A and a small increase in b (Rosenfeld and Ulbrich, 2003). All of these facts were not observed in the RSD (Fig. 2) and gamma parameters (Fig. 5). Thus, breakup

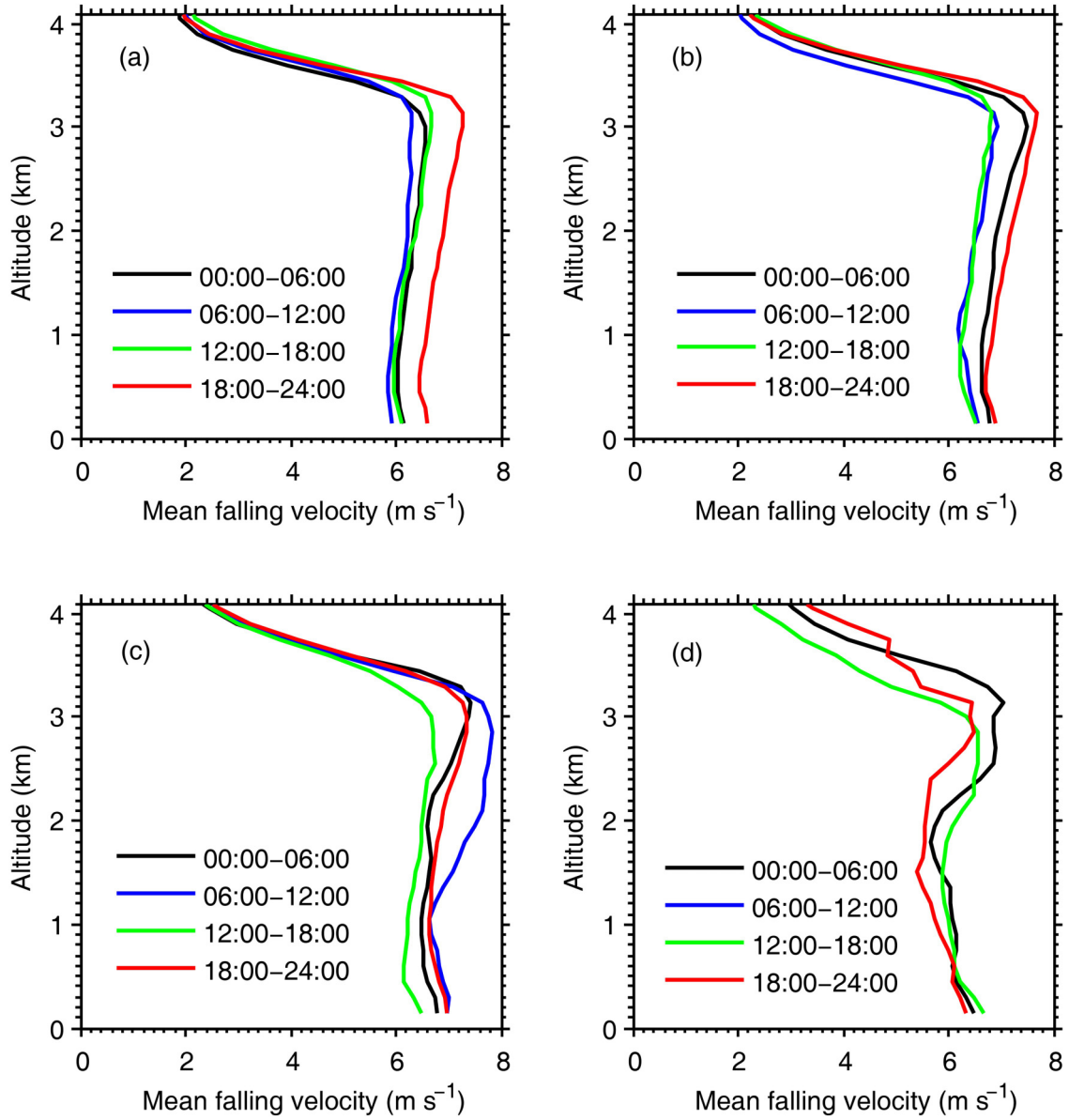

Fig. 7. As in Fig. 6 but for mean falling velocity.

is not the dominant process affecting the RSD of stratiform rain at Kototabang.

Updrafts may also cause a decrease in the number of small drops by carrying small raindrops to higher altitudes (Seela et al., 2017). Marzuki et al. (2016a) analyzed updrafts at Kototabang using vertical wind data from EAR observations. We classified the data in Marzuki et al. (2016a) on a diurnal basis (figure not shown). A stronger updraft was observed during 1200–2400 LST, but the difference in the updraft strength for each time period at Kototabang was small and may not have caused any significant difference in the RSD. Furthermore, the updrafts during stratiform rain are weak and only strong updrafts can lift large hydrometeors to higher altitudes (Heymsfield et al., 2010).

Apart from RSD (Fig. 4), the role of collision–coalescence can also be seen from the vertical profile of Z. The role of collision–coalescence can be observed from the Z gradient in the rain column (0.45–3 km AGL) (Fig. 6). Because Z is proportional to D^6, it is therefore more sensitive to large drops. Accordingly, a downward increase in Z may indicate a downward increase in large drop numbers, especially in heavy rain. Figure 11 shows the mean vertical profile of Z at Kototabang from TRMM PR 2A25 during 2012–15. A more positive gradient was observed during 1200–1800 LST, particularly for moderate and heavy rains, which indicates more raindrop growth due to collision–coalescence than at the other times. The consequence of coalescence is D_m must increase and N_T must decrease. Furthermore, coalescence also causes an increase in A and small decrease in b of the Z–R relation (Rosenfeld and Ulbrich, 2003). A similar pattern was obtained in this work, particularly for moderate and heavy rains (Figs. 5 and 9). While the growth of raindrops due to collision–coalescence was likely stronger during 1200–1800 LST, a higher D_m at the

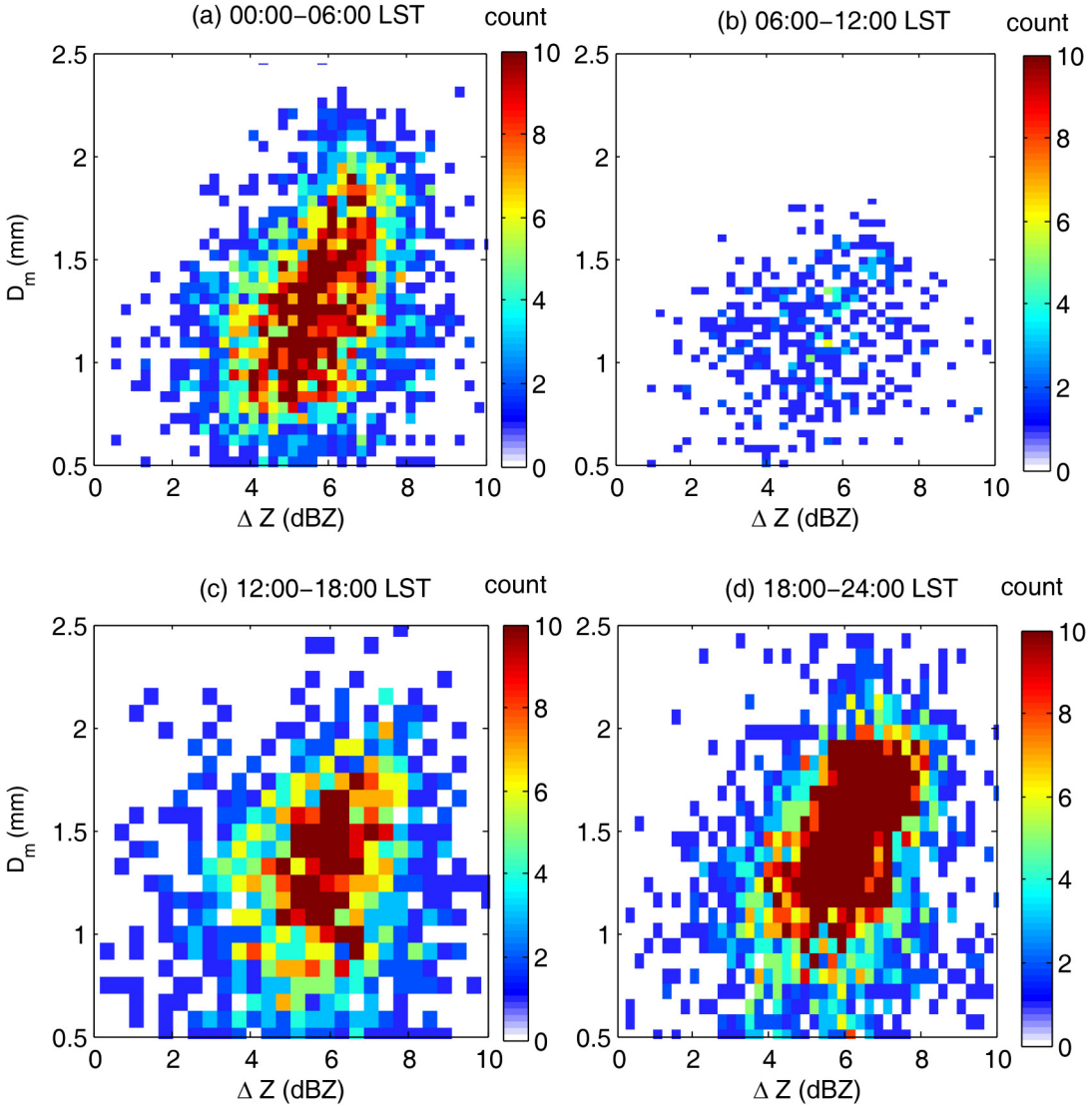

Fig. 8. Relationship between ΔZ and D_m for the altitude of 0.45 km, on a diurnal basis.

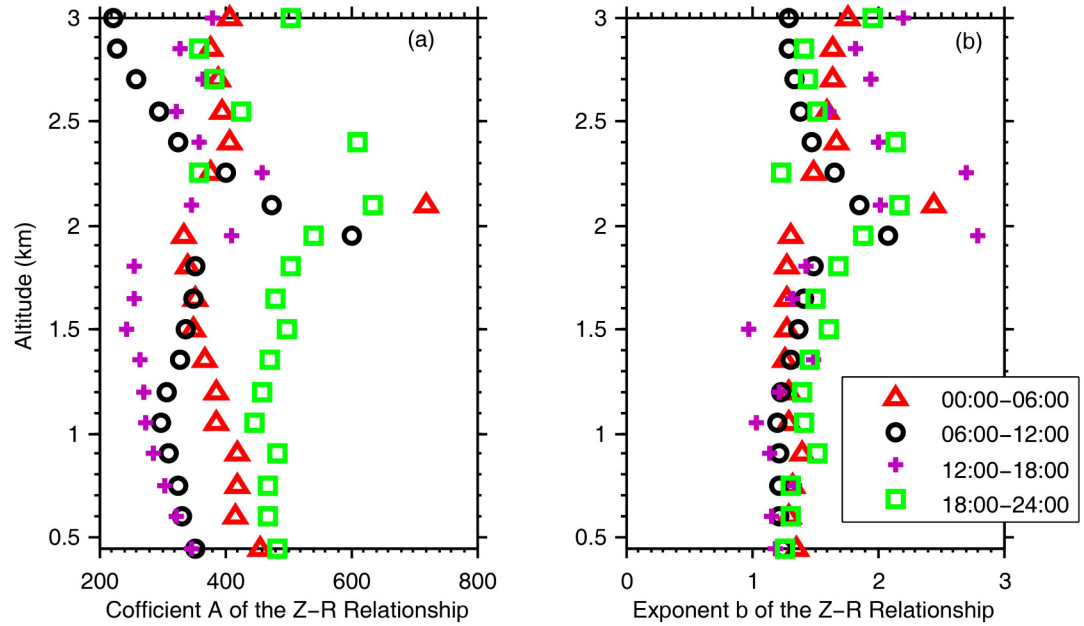

Fig. 9. Vertical distribution of (a) coefficient A and (b) coefficient b of the Z–R relationship on diurnal basis.

ground surface was observed during 0000–0600 and 1800–2400 LST (Fig. 5). The large raindrops during 0000–0600 and 1800–2400 LST were likely the result of the melting of the larger snowflake aggregates with minimal breakup. In addition to Fig. 8, a stronger BB during 0000–0600 and 1800–2400 LST can be clearly observed from Fig. 11, as indicated by the larger maximum Z in the BB. Furthermore, just below the BB (3.0–2.5 km), the value of Z during 0000–0600 and 1800–2400 LST was also larger than that during 1200–1800 LST.

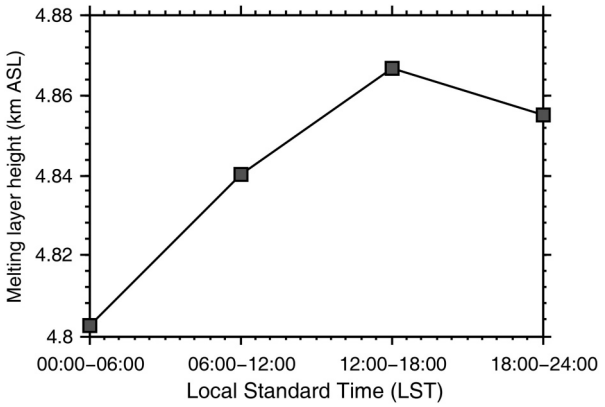

Fig. 10. Mean melting layer height at Kototabang in km above sea level from TRMM PR 2A25 during 2012–15.

4. Conclusions

The vertical structure of the RSD of stratiform rain at Kototabang shows strong diurnal variation. The concentration of raindrops in the afternoon (1200–1800 LST) is much larger than those at other times. Moreover, the RSD in the afternoon consists of a larger concentration of small drops and a lower concentration of large drops. This difference is due to the differences in the growth process of the raindrops. During the period 1200–1800 LST, the riming process is dominant, whereas aggregation is dominant in the morning (0000–0600 LST), which can be inferred from the BB strength. In addition, the differences are also due to the

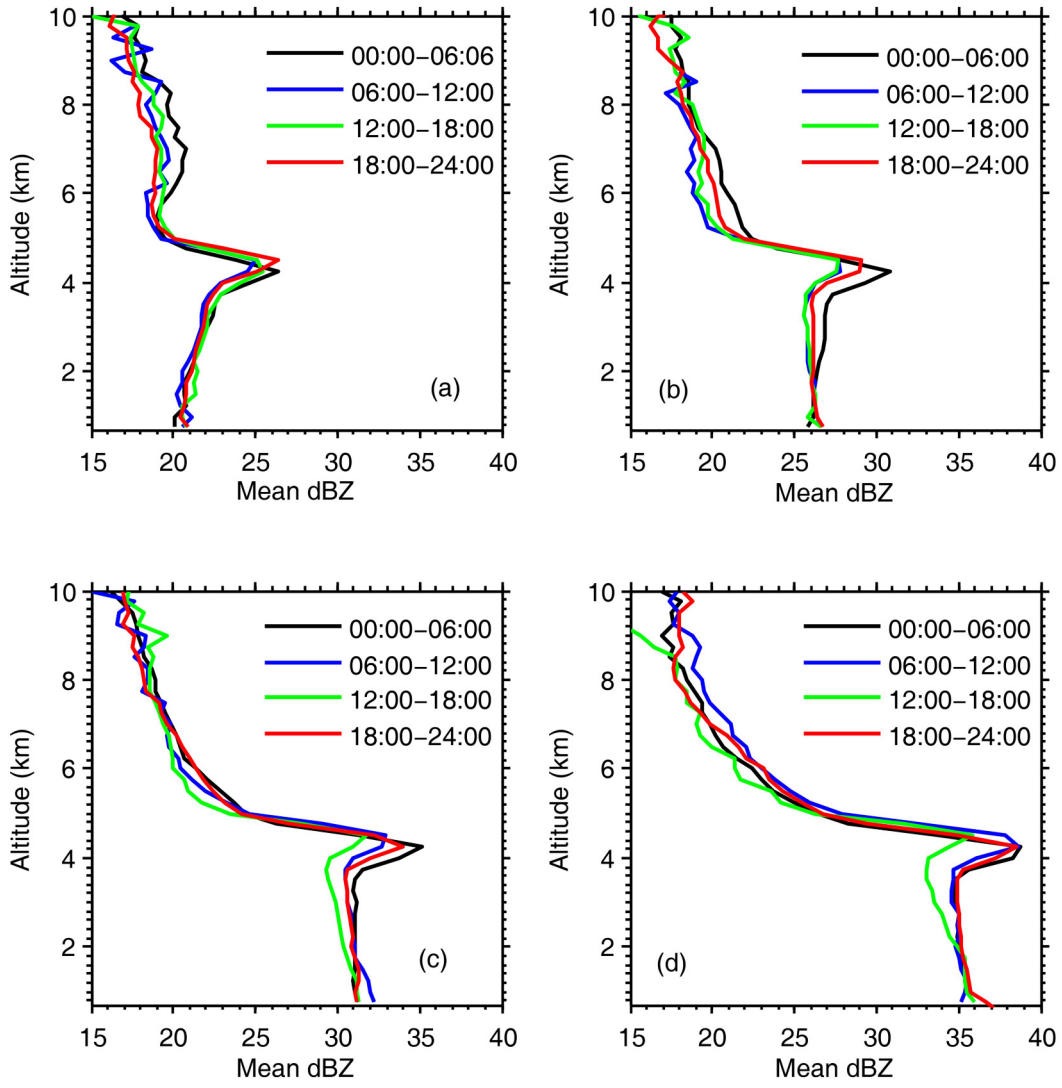

Fig. 11. Mean vertical profile of Z at Kototabang from TRMM PR 2A25 during 2012–15.

differences in the evolution of the raindrops. Besides spontaneous growth, coalescence seems to occur at all intensities of stratiform rain at Kototabang. The diurnal variation in the vertical profile of the RSD has an impact on the rainfall estimate obtained with weather radar. Coefficient A of the Z–R relation decreases with decreasing altitude, and the smallest value is observed during the period 1200–1800 LST. Thus, estimation of R using a fixed Z–R relation can result in large errors, even for stratiform rain.

Acknowledgements. This study was supported by the 2019 Basic Research Grants from the Ministry of Research, Technology and Higher Education (Grant No. T/3/UN.16.17/PT.01.03/PD-Kebencanaan/2019). The observations made by the MRR at Kototabang during the rain event were supported by RISH, Kyoto University.

REFERENCES

Albright, M. D., D. R. Mock, E. E. Recker, and R. J. Reed, 1981: A diagnostic study of the diurnal rainfall variation in the GATE B-scale area. *J. Atmos. Sci.*, **38**, 1429–1445, https://doi.org/10.1175/1520-0469(1981)038<1429:ADSOTD>2.0.CO;2.

Albright, M. D., E. E. Recker, R. J. Reed, and R. Q. Dang, 1985: The diurnal variation of deep convection and inferred precipitation in the central tropical Pacific during January-February 1979. *Mon. Wea. Rev.*, **113**, 1663–1680, https://doi.org/10.1175/1520-0493(1985)113<1663:TDVODC>2.0.CO;2.

Aldrian, E., and R. Dwi Susanto, 2003: Identification of three dominant rainfall regions within Indonesia and their relationship to sea surface temperature. *International Journal of Climatology*, **23**, 1435–1452, https://doi.org/10.1002/joc.950.

Atlas, D., R. C. Srivastava, and R. S. Sekhon, 1973: Doppler radar characteristics of precipitation at vertical incidence. *Rev. Geophys.*, **11**, 1–35, https://doi.org/10.1029/RG011i001p00001.

Augustine, J. A., 1984: The diurnal variation of large-scale inferred rainfall over the tropical Pacific Ocean during August 1979. *Mon. Wea. Rev.*, **112**, 1745–1751, https://doi.org/10.1175/1520-0493(1984)112<1745:TDVOLS>2.0.CO;2.

Cifelli, R., C. R. Williams, D. K. Rajopadhyaya, S. K. Avery, K. S. Gage, and P. T. May, 2000: Drop-size distribution characteristics in tropical mesoscale convective systems. *J. Appl. Meteorol.*, **39**, 760–777, https://doi.org/10.1175/1520-0450(2000)039<0760:DSDCIT>2.0.CO;2.

Fabry, F., and I. Zawadzki, 1995: Long-term radar observations of the melting layer of precipitation and their interpretation. *J. Atmos. Sci.*, **52**, 838–851, https://doi.org/10.1175/1520-0469(1995)052<0838:LTROOT>2.0.CO;2.

Fukao, S., and Coauthors, 2003: Equatorial Atmosphere Radar (EAR): System description and first results. *Radio Sci.*, **38**, 1053, https://doi.org/10.1029/2002RS002767.

Geerts, B., and T. Dejene, 2015: Regional and diurnal variability of the vertical structure of precipitation systems in Africa based on spaceborne radar data. *J. Climate*, **18**, 893–916, https://doi.org/10.1175/JCLI-3316.1.

Hamilton, K., 1981: A note on the observed diurnal and semidiurnal rainfall variations. *J. Geophys. Res.*, **86**, 12, https://doi.org/10.1029/JC086iC12p12122.

Heymsfield, G. M., L. Tian, A. J. Heymsfield, L. H. Li, and S. Guimond, 2010: Characteristics of deep tropical and subtropical convection from nadir-viewing high-altitude airborne Doppler radar. *J. Atmos. Sci.*, **67**, 285–308, https://doi.org/10.1175/2009JAS3132.1.

Hu, Z. L., and R. C. Srivastava, 1995: Evolution of raindrop size distribution by coalescence, breakup, and evaporation: Theory and observations. *J. Atmos. Sci.*, **52**, 1761–1783, https://doi.org/10.1175/1520-0469(1995)052<1761:EORSDB>2.0.CO;2.

Huggel, A., W. Schmid, and A. Waldvogel, 1996: Raindrop size distributions and the radar bright band. *J. Appl. Meteorol.*, **35**, 1688–1701, https://doi.org/10.1175/1520-0450(1996)035<1688:RSDATR>2.0.CO;2.

Kozu, T., and K. Nakamura, 1991: Rainfall parameter estimation from dual-radar measurements combining reflectivity profile and path-integrated attenuation. *J. Atmos. Oceanic Technol.*, **8**, 259–270, https://doi.org/10.1175/1520-0426(1991)008<0259:RPEFDR>2.0.CO;2.

Kozu, T., K. K. Reddy, S. Mori, M. Thurai, J. T. Ong, D. N. Rao, and T. Shimomai, 2006: Seasonal and diurnal variations of raindrop size distribution in Asian monsoon region. *J. Meteorol. Soc. Japan*, **84A**, 195–209, https://doi.org/10.2151/jmsj.84A.195.

Kozu, T., T. Shimomai, Z. Akramin, Marzuki, Y. Shibagaki, and H. Hashiguchi, 2005: Intraseasonal variation of raindrop size distribution at Koto Tabang, West Sumatra, Indonesia. *Geophys. Res. Lett.*, **32**, L07803, https://doi.org/10.1029/2004GL022340.

Kumjian, M. R., and A. V. Ryzhkov, 2010: The impact of evaporation on polarimetric characteristics of rain: Theoretical model and practical implications. *J. Appl. Meteorol. Climatol.*, **49**, 1247–1267, https://doi.org/10.1175/2010JAMC2243.1.

Lee, G. W., and I. Zawadzki, 2005: Variability of drop size distributions: Noise and noise filtering in disdrometric data. *J. Appl. Meteorol.*, **44**, 634–652, https://doi.org/10.1175/JAM2222.1.

Li, X. W., and R. C. Srivastava, 2001: An analytical solution for raindrop evaporation and its application to radar rainfall measurements. *J. Appl. Meteorol.*, **40**, 1607–1616, https://doi.org/10.1175/1520-0450(2001)040<1607:AASFRE>2.0.CO;2.

Marzuki, T. Kozu, T. Shimomai, W. L. Randeu, H. Hashiguchi, and Y. Shibagaki, 2009: Diurnal variation of rain attenuation obtained from measurement of raindrop size distribution in equatorial Indonesia. *IEEE Trans. Antennas Propag.*, **57**(4), 1191–1196, https://doi.org/10.1109/TAP.2009.2015812.

Marzuki, H. Hashiguchi, T. Kozu, T. Shimomai, Y. Shibagaki, and Y. Takahashi, 2016a: Precipitation microstructure in different Madden-Julian Oscillation phases over Sumatra. *Atmospheric Research*, **168**, 121–138, https://doi.org/10.1016/j.atmosres.2015.08.022.

Marzuki, H. Hashiguchi, T. Shimomai, and W. L. Randeu, 2016b: Cumulative distributions of rainfall rate over Sumatra. *Progress in Electromagnetics Research M*, **49**, 1–8, https://doi.org/10.2528/PIERM16043007.

Marzuki, H. Hashiguchi, T. Shimomai, I. Rahayu, M. Vonnisa, and Afdal, 2016c: Performance evaluation of Micro Rain Radar over Sumatra through comparison with disdrometer and wind profiler. *Progress in Electromagnetics Research M*, **50**, 33–46, https://doi.org/10.2528/PIERM16072808.

Marzuki, H. Hashiguchi, M. Vonnisa, Harmadi, and M. Katsumata, 2018a: Determination of intraseasonal variation of precipitation microphysics in the Southern Indian Ocean from Joss-Waldvogel Disdrometer observation during the CINDY Field Campaign. *Adv. Atmos. Sci.*, **35**(11), 1415–1427, https://doi.org/10.1007/s00376-018-8026-5.

Marzuki, H. Hashiguchi, M. Vonnisa, Harmadi, and Muzirwan, 2018b: Long-term change in rainfall rate and melting layer height in Indonesia. *Proc. 2018 Progress in Electromagnetics Research Symposium*, Toyama, IEEE, https://doi.org/10.23919/PIERS.2018.8597606.

Marzuki, H. Hashiguchi, M. Vonnisa, Harmadi, Muzirwan, S. Nugroho, and M. Yoseva, 2018c: Z-R relationships for weather radar in Indonesia from the particle size and velocity (Parsivel) optical disdrometer. *Proc. Progress in Electromagnetics Research Symposium*, Toyama, IEEE, https://doi.org/10.23919/PIERS.2018.8597693.

Marzuki, H. Hashiguchi, M. Vonnisa, and Harmadi, 2018d: Seasonal and diurnal variations of vertical profile of precipitation over Indonesian maritime continent, engineering and mathematical topics in rainfall. Theodore V Hromadka II and Prasada Rao, Eds., IntechOpen. https://doi.org/10.5772/intechopen.74044.

Marzuki, T. Kozu, T. Shimomai, H. Hashiguchi, W. L. Randeu, and M. Vonnisa, 2010: Raindrop size distributions of convective rain over equatorial Indonesia during the first CPEA campaign. *Atmospheric Research*, **96**, 645–655, https://doi.org/10.1016/j.atmosres.2010.03.002.

Marzuki, W. L. Randeu, T. Kozu, T. Shimomai, H. Hashiguchi, and M. Schönhuber, 2013a: Raindrop axis ratios, fall velocities and size distribution over Sumatra from 2D-Video Disdrometer measurement. *Atmospheric Research*, **119**, 23–37, https://doi.org/10.1016/j.atmosres.2011.08.006.

Marzuki, M., H. Hashiguchi, M. K. Yamamoto, S. Mori, and M. D. Yamanaka, 2013b: Regional variability of raindrop size distribution over Indonesia. *Annales Geophysicae*, **31**, 1941–1948, https://doi.org/10.5194/angeo-31-1941-2013.

Mori, S., H. Jun-Ichi, Y. I. Tauhid, M. D. Yamanaka, N. Okamoto, F. Murata, N. Sakurai, H. Hashiguchi, and T. Sribimawati, 2004: Diurnal land-sea rainfall peak migration over Sumatera island, Indonesian maritime continent, observed by TRMM satellite and intensive rawinsonde soundings. *Mon. Wea. Rev.*, **132**, 2021–2039, https://doi.org/10.1175/1520-0493(2004)132<2021:DLRPMO>2.0.CO;2.

Nauval, F., Marzuki, and H. Hashiguchi, 2017: Regional and diurnal variations of rain attenuation obtained from measurement of raindrop size distribution over Indonesia at Ku, Ka and W Bands. *Progress in Electromagnetics Research M*, **57**, 25–34, https://doi.org/10.2528/PIERM17030503.

Peters, G., B. Fischer, H. Münster, M. Clemens, and A. Wagner, 2005: Profiles of raindrop size distributions as retrieved by microrain radars. *J. Appl. Meteorol.*, **44**, 1930–1949, https://doi.org/10.1175/JAM2316.1.

Radhakrishna, B., T. N. Rao, D. N. Rao, N. P. Rao, K. Nakamura, and A. K. Sharma, 2009: Spatial and seasonal variability of raindrop size distributions in southeast India. *J. Geophys. Res.*, **114**, D04203, https://doi.org/10.1029/2008JD011226.

Renggono, F., M. K. Yamamoto, H. Hashiguchi, S. Fukao, T. Shimomai, M. Kawashima, and M. Kudsy, 2006: Raindrop size distribution observed with the Equatorial Atmosphere Radar (EAR) during the Coupling Processes in the Equatorial Atmosphere (CPEA-I) observation campaign. *Radio Sci.*, **41**, RS5002, https://doi.org/10.1029/2005RS003333.

Rosenfeld, D., and C. W. Ulbrich, 2003: Cloud microphysical properties, processes, and rainfall estimation opportunities. *Radar and Atmospheric Science: A Collection of Essays in Honor of David Atlas*, R. M. Wakimoto and R. Srivastava, Eds., American Meteorological Society, 237–258, https://doi.org/10.1007/978-1-878220-36-3_10.

Sarma, A. C., A. Deshamukhya, T. N. Rao, and S. Sharma, 2016: A study of raindrop size distribution during stratiform rain and development of its parameterization scheme in the framework of multi-parameter observations. *Meteorological Applications*, **23**, 254–268, https://doi.org/10.1002/met.1551.

Schumacher, C., and R. A. Houze Jr., 2003: Stratiform rain in the Tropics as seen by the TRMM precipitation radar. *J. Climate*, **16**, 1739–1756, https://doi.org/10.1175/1520-0442(2003)016<1739:SRITTA>2.0.CO;2.

Seela, B. K., J. Janapati, P. L. Lin, K. K. Reddy, R. Shirooka, and P. K. Wang, 2017: A comparison study of summer season raindrop size distribution between Palau and Taiwan, two islands in western Pacific. *J. Geophys. Res.*, **122**(11), 11 787–11 805, https://doi.org/10.1002/2017JD026816.

Sui, C. H., K. M. Lau, Y. N. Takayabu, and D. A. Short, 1997: Diurnal variations in tropical oceanic cumulus convection during TOGA COARE. *J. Atmos. Sci.*, **54**, 639–655, https://doi.org/10.1175/1520-0469(1997)054<0639:DVITOC>2.0.CO;2.

Tian, B. J., B. J. Soden, and X. Q. Wu, 2004: Diurnal cycle of convection, clouds, and water vapor in the tropical upper troposphere: Satellites versus a general circulation model. *J. Geophys. Res.*, **109**, D10101, https://doi.org/10.1029/2003JD004117.

Tokay, A., and D. A. Short, 1996: Evidence from tropical raindrop spectra of the origin of rain from stratiform versus convective clouds. *J. Appl. Meteorol.*, **35**, 355–371, https://doi.org/10.1175/1520-0450(1996)035<0355:EFTRSO>2.0.CO;2.

Tokay, A., W. A. Petersen, P. Gatlin, and M. Wingo, 2013: Comparison of raindrop size distribution measurements by collocated disdrometers. *J. Atmos. Oceanic Technol.*, **30**, 1672–1690, https://doi.org/10.1175/JTECH-D-12-00163.1.

Ushiyama, T., K. K. Reddy, H. Kubota, K. Yasunaga, and R. Shirooka, 2009: Diurnal to interannual variation in the raindrop size distribution over Palau in the western tropical Pacific. *Geophys. Res. Lett.*, **36**, L02810, https://doi.org/10.1029/2008GL036242.

Wang, H., H. C. Lei, and J. F. Yang, 2017: Microphysical processes of a stratiform precipitation event over Eastern China: Analysis using micro rain radar data. *Adv. Atmos. Sci.*, **34**(12), 1472–1482, https://doi.org/10.1007/s00376-017-7005-6.

Wilson, J. W., and E. A. Brandes, 1979: Radar measurement of rainfall—A summary. *Bull. Amer. Meteorol. Soc.*, **60**, 1048–1060, https://doi.org/10.1175/1520-0477(1979)060<1048:RMORS>2.0.CO;2.

Yang, G. Y., and J. Slingo, 2001: The diurnal cycle in the tropics. *Mon. Wea. Rev.*, **129**, 784–801, https://doi.org/10.1175/1520-0493(2001)129<0784:TDCITT>2.0.CO;2.

Zawadzki, I., W. Szyrmer, C. Bell, and F. Fabry, 2005: Modeling of the melting layer. Part III: The density effect. *J. Atmos. Sci.*, **62**, 3705–3723, https://doi.org/10.1175/JAS3563.1.